Island phases and charge order in two-dimensional manganites

H. Aliaga,[1] B. Normand,[2] K. Hallberg,[1] M. Avignon,[3] and B. Alascio[1]
[1]*Instituto Balseiro and Centro Atomico Bariloche, Comision Nacional de Energia Atomica, 8400 San Carlos de Bariloche, Argentina*
[2]*Theoretische Physik III, Elektronische Korrelationen und Magnetismus, Institut für Physik, Universität Augsburg, D-86135 Augsburg, Germany*
[3]*Laboratoire d'Etudes des Propriétés Electroniques des Solides (LEPES), Centre National de la Récherche Scientifique, BP 166, F-38042 Grenoble Cedex, France*
(Received 22 November 2000; published 21 June 2001)

The ferromagnetic Kondo lattice model with an antiferromagnetic interaction between localized spins is a minimal description of the competing kinetic (t) and magnetic (K) energy terms which generate the rich physics of manganite systems. Motivated by the discovery in one dimension of homogeneous ''island phases,'' we consider the possibility of analogous phases in higher dimensions. We characterize the phases present at commensurate fillings, and consider in detail the effects of phase separation in all filling and parameter regimes. We deduce that island and flux phases are stable for intermediate values of K/t at the commensurate fillings $n=1/4$, 1/3, 3/8, and 1/2. We discuss the connection of these results to the charge and magnetic ordering observed in a wide variety of manganite compounds.

DOI: 10.1103/PhysRevB.64.024422 PACS number(s): 75.10.−b, 75.30.Vn, 75.40.Mg

I. INTRODUCTION

Transition-metal manganite compounds have long been known to display a broad spectrum of physical properties as a function of temperature, filling, and counterion composition. While the most remarkable of these is the colossal magnetoresistance[1] observed in the ferromagnetic (FM) phase, the phase diagrams of both cubic perovskite and layered manganite materials exhibit a rich variety of metallic, insulating, magnetically ordered, and, apparently, inhomogeneous or phase-separated regions.

The ferromagnetic Kondo lattice model (FKLM) has been used extensively as a minimal model to reproduce the physics responsible for this situation. We will study a version of the model which includes a Heisenberg interaction between the localized spins. In essence, this encapsulates the competition between the ferromagnetic polarizing effect of the double-exchange hopping term[2] (t) for mobile carriers in the e_g orbitals of Mn^{3+}, and the antiferromagnetic (AF) interaction (K) between the localized spins composed of electrons in the t_{2g} orbitals. Treatments of the model with both classical local spins, and with fully quantum, $S=1/2$ local spins, both return some of the features observed among the selection of manganite phase diagrams. A large number of authors has worked on many forms of the FKLM, and we will present in the following sections only a small selection of references relevant to the current approach.

Following the discovery[3] in one-dimensional simulations of novel ''island phases'' near commensurate values of electron filling in the FKLM with strong Hund coupling between localized and conduction electrons, we wish here to consider the possibility of higher-dimensional generalizations of these phases. By an island phase is meant a spin configuration composed of small, regularly arranged, FM islands (clusters of 2–4 sites in Ref. 3), with AF local spin orientations between islands (Fig. 1). These phases are homogeneous, and near the commensurate fillings maximize kinetic energy within each island at minimal cost to the magnetic energy, which is favored at the island boundaries. Focusing primarily on the problem in two dimensions (2D), we wish to establish the possibility that such islands, which may be small in one or both directions, remain the most stable phase for certain fillings and parameter ratios K/t.

A particular motivation for our study is the recent observation of charge-ordering phenomena, and more general inhomogeneous charge and spin configurations, in a variety of manganite systems. These appear in both layered and cubic materials, and at both commensurate and incommensurate values of the electron filling set by the counterion doping. Some of the earliest observations of charge ordering[4] were made in $La_{1-x}Sr_xMnO_3$, and were followed by measurements suggesting polarons,[5] phase separation,[6] and paired stripe features.[7] Charge order coupled to a structural phase transition has been observed in $Bi_{1-x}Ca_xMnO_3$ at incommensurate values of the filling x.[8,9] Among hole-doped manganites, charge ordering arose at incommensurate filling in $Nd_{1-x}Sr_xMnO_3$, and in a stripelike configuration at half-filling in $Pr_{0.5}Sr_{0.5}MnO_3$.[10,11] For the latter system, the stripe features could be made to ''melt'' in an applied magnetic field.[10] Of most interest in the current context, ordering phenomena have also appeared in 2D or layered manganite systems. In $Sr_{2-x}La_xMnO_3$ at low doping, Bao *et al.*[12] reported charge order, phase separation, and triplet bipolarons. For the

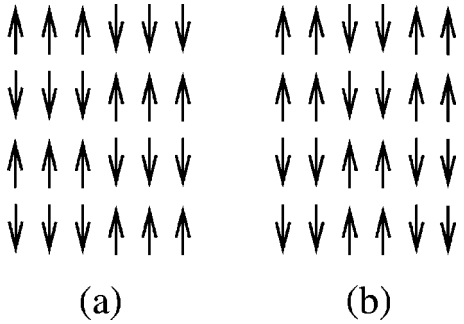

FIG. 1. Schematic representations of the island phases $(\pi/3,\pi)$ (a) and $(\pi/2,\pi/2)$ (b).

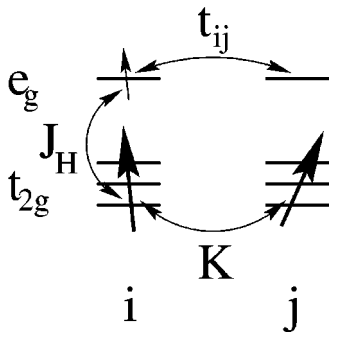

FIG. 2. Schematic representation of the Hamiltonian (1) for two sites.

same system at $x=0.5$, Moritomo *et al.*[13] related charge ordering to lattice effects by substitution for La, and Murakami *et al.*[14] made direct measurements of charge and orbital order for the commensurate La member. Finally, we mention also the observation[15] of charge order in the layered 327 compound $LaSr_2Mn_2O_7$.

The paper is organized as follows. In Sec. II we present the model in the form we wish to consider, and outline the methods by which it is analyzed. In Sec. III we discuss the available means to characterize the phases which appear, and illustrate these with examples. Section IV contains a detailed discussion of the issue of phase separation, and a global phase diagram for the augmented FKLM which delimits the regimes of interest for island phases. We return in Sec. V to the robust flux and island phases, discuss their properties and their charge order, and consider their relevance to the above experiments. Section VI gives a summary and conclusions.

II. MODEL AND METHODS

We consider the FKLM in the form

$$H=-\sum_{\langle ij\rangle\sigma} t_{ij}(c_{i\sigma}^{\dagger}c_{i\sigma}+\text{H.c.})-J_H\sum_i \mathbf{s}_i\cdot\mathbf{S}_i+K\sum_{\langle ij\rangle}\mathbf{S}_i\cdot\mathbf{S}_j, \tag{1}$$

as represented schematically in Fig. 2. Here $c_{i\sigma}^{\dagger}$ is the operator creating an electron of spin σ in the sole e_g orbital; $\mathbf{s}_i=\Sigma_{\alpha\beta}c_{i\alpha}^{\dagger}\sigma_{\alpha\beta}c_{i\beta}$ gives the spin of this ''conduction'' electron, and its mobility depends on the orientation of the localized t_{2g} spins according to the double-exchange mechanism.[2] The second term is the Hund coupling, $J_H>0$, which favors a FM orientation of spins on the same site. Following Refs. 16,17, we will be concerned with the limit of large J_H; while in real systems J_H is of the same order as the bandwidth, this simplifying approximation has been found to give reasonable results. The limit corresponds to a situation where the conduction electron is bound to follow the spin texture of the localized system, while antialigned electrons occupy a band with energy higher by J_H. The projecting effect of the large Hund coupling allows one to neglect direct Coulomb interactions of the e_g electrons. The final term, with $K>0$, expresses the AF interactions between the local t_{2g} spins, whose competition with the FM spin alignment required to maximize e_g electron kinetic energy (2) generates the intrinsic physics of interest in the context of manganite materials.

In the following we will consider the properties of the model (1) over the full parameter range. Bare values of the ratio K/t deduced to date for real systems are rather small. A recent study of the double-exchange phase diagram (see Ref. 18, and references therein) outlines this situation for the (La,Ca)MnO_3 system, and summarizes the reasons (e_g electron contributions, direct exchange enhancement) why the measured ratio $K/t\simeq 0.005$ may be raised to effective values on the order of 0.1. We note further that the manganese perovskite structure offers a wide variety of counterions, and systems such as (Bi,Ca)MnO_3 (Ref. 8) have a significantly smaller lattice constant than (La,Ca)MnO_3. This may be expected to give rise to a marked increase in the ratio K/t, and indeed superexchange values (12.6 meV) larger by a factor of 20 have been found in the former compound.[8] Thus K/t values in excess of 0.2 would appear to be physically reasonable.

We will analyze the model primarily by a classical Monte Carlo (MC) procedure for the localized spins, in conjunction with exact diagonalization of the conduction electron system.[19,20] The localized spins are thus taken to be classical, an approximation to the true situation of $S=3/2$ which is found not to invalidate the connection to real systems. The conduction electrons are taken to occupy a single e_g orbital, or band, and from the condition on J_H only one spin projection need be considered. This part of the process is the solution of the single-electron problem with hopping set consistently by the localized spin configuration. In the limits of large S and J_H, this is[16]

$$t_{ij}=t\left(\cos\frac{\theta_i}{2}\cos\frac{\theta_j}{2}+e^{-(\phi_i-\phi_j)}\sin\frac{\theta_i}{2}\sin\frac{\theta_j}{2}\right), \tag{2}$$

where θ_i and ϕ_i are the polar angles of spin $\mathbf{S}_i$. The resulting energy levels are then filled by the available number of electrons in the canonical ensemble.

The MC simulation proceeds from the FKLM partition function with classical spins,

$$Z=\prod_{i=1}^{N\times N}\int_0^{\pi}d\theta_i\sin\theta_i\int_0^{2\pi}d\phi_i\,\text{Tr}[\exp(-\beta H)], \tag{3}$$

where N is the system dimension. Positivity of the integrand assures that the sign problem is absent. Updates of the spin configuration $\{\theta_i,\phi_i\}$ are accepted or rejected according to the Glauber algorithm. In simulations with these spherical angles we were unable to find in the 2D system any cases where noncoplanar spin configurations appear. Because of the large degeneracy of coplanar phases, the simulations could be accelerated by fixing $\theta_i=\pi/2$, and varying only the angles $\{\phi_i\}$. The number of MC steps per site for $N=8$ is taken as 2000 to equilibrium and 3000 for measurement, while for $N=12$ the corresponding numbers are 500 and 1000. The equilibrium criterion was taken from the number of steps required to ensure a relative standard deviation on the energies per site smaller than 5×10^{-4}. Systems of size up to 12×12 are accessible by this method, and thus we

supplement the MC results by a variety of classical analytical considerations, which afford considerable insight and allow a detailed assessment of finite-size effects. The simulations may be pursued down to temperatures of $T=0.005t$, which unless otherwise stated will be the relevant value for the MC results displayed. This temperature is sufficiently low that comparison with the zero temperature, analytical calculations is meaningful, and in most cases quantitatively so. The method is the same as that used by Dagotto, Yunoki, and co-workers in a series of papers.[19–24] We will reproduce some of the same results, and comment on the similarities and differences in the context of our island phase analyses in what follows.

Because the classical MC method has been used before in the literature, we comment only briefly on further technical issues in order to focus on the physics of the model. In all cases the boundary conditions used were periodic. Finite-size effects are known to be very strong for small clusters (4×4, 6×6), and we will show only results for the larger systems (8×8, 12×12) which we believe from commensurability and comparison with the infinite system to be representative for the phases illustrated. We performed simulations using a variety of initial spin configurations; while the most unbiassed starting point is a paramagnetic (PM) spin configuration, convergence in this case may be very long. The majority of our simulations at the lowest temperatures illustrated here were performed with a starting state obtained from MC at a higher temperature. This ensured convergence in a reasonable number of steps, and agreed in all cases we tested with the results from the PM start. Finally, we have obtained data over a range of temperatures with a view to analyzing the thermodynamic properties of the model. While finite temperatures may stabilize interesting excited spin states, further expanding the space of configurations to be discussed below,[25] we will restrict our considerations here to the ground-state properties of the model (1).

III. PHASE CHARACTERIZATION

In this section we will present some results for typical phases which emerge from MC simulations performed at the commensurate fillings $n=1/2$, 1/3, and 1/4, and for the full range of values of K/t. The results of the simulations for the localized spin system may be characterized by three separate but related quantities: the spin structure factor

$$S(\mathbf{k})=\sum_{i,j}\ \mathbf{S}_i\cdot\mathbf{S}_j e^{i\mathbf{k}(\mathbf{r}_i-\mathbf{r}_j)}, \tag{4}$$

a histogram of the distribution of angles between all nearest-neighbor spin pairs, which we choose to present as a function of $\cos\Theta_{ij}$, and a simple ''snapshot'' of the spin configurations at a representative step late in the MC process. Note for the histogram that Θ_{ij} is the full angle between spins given by $\cos\Theta_{ij}=(\mathbf{S}_i\cdot\mathbf{S}_j)/S^2$ for the classical case, and is not to be confused with the on-site azimuthal angle θ_i in Eq. (2). Finally, one may compute in addition the charge distribution function

$$n(\mathbf{k})=\sum_i\ n_i e^{i\mathbf{k}\cdot\mathbf{r}_i}, \tag{5}$$

and [by analogy with Eq. (4)] the charge-charge correlation function $N(\mathbf{k})$, which we will use in Sec. V when considering charge order.

As a guide to understand the variety of possibilities which is contained in these quantities, we first calculate the classical, ground-state energies of a multiplicity of possible spin configurations. This may be carried out for an infinite 2D system by straightforward extension from the arguments presented for the 1D case in Ref. 3. For each spin configuration, the magnetic energy per spin is a simple function of the average of the angles across each bond, which varies from $2K$ for the FM case to $-2K$ for the AF. The kinetic energy at this level is a readily calculable function of the spin configuration which varies from 0 in the AF case, where all kinetic processes are excluded, to the average energy of the 2D nearest-neighbor band $\epsilon_k=-2t(\cos k_x+\cos k_y)$, for the relevant band filling, in the FM case where it is maximally negative. The results of this exercise are illustrated in Fig. 3 for $n=1/2$, $n=1/3$, and $n=1/4$.

All of the phases denoted by $(k\pi/m,l\pi/m)$ have neighboring spins only either parallel or antiparallel, in both directions. The rational fractions $k/m,l/m$ may be understood as indicating that the spin direction turns over k or l times in $2m$ lattice constants. Figure 1 shows two small-m possibilities, the $(\pi/3,\pi)$ (a) and $(\pi/2,\pi/2)$ (b) phases. As a more complex example, the phase $(3\pi/4,\pi)$, which appears over a wide range of K/t at filling $n=1/4$ [Figs. 3(c),6], would be composed of chains with repeat unit $\uparrow\uparrow\downarrow\uparrow\downarrow\downarrow\uparrow\downarrow$ in the x direction, and AF alignment in the y direction. In addition to these phases, which include the FM (0,0) and AF (π,π) end points, we include also the ''flux phase,''[26,24] which will be discussed in more detail below, and a ''double spiral'' (DS) phase, by which is meant a single phase where the nearest-neighbor spins rotate by the same angle $0\leqslant\Theta\leqslant\pi$ in both x and y directions. In this last case, the optimal angle Θ is obtained by minimizing a function of K/t, and the double spiral may be expected to be more favorable than any variety of single-spiral phases combined with other forms of modulation in the transverse direction. Although we have considered many possible phases of the above types, in Fig. 3 we include for clarity only those which are the ground state for some range of K/t.

The calculation of all of these phase energies is straightforward. In brief, calculation of the only 2D band at (0,0) proceeds as above, with the filling determining the chemical potential up to which the filled band is integrated. For the 1D structures $(0,l\pi/m)$, one may consider the band $\epsilon_k=-2t\cos k$ in the continuous direction, split appropriately into 2, 3, or 4 (the maximum included here) by an equal interchain hopping t. Integration over the filled parts of these bands up to the chemical potential yields the average kinetic energy. For the ''0D'' structures $(k\pi/m,l\pi/m)$, the kinetic energy is a simple m^2/kl-site diagonalization problem to obtain the discrete levels. These phases are particularly favorable when the filling exactly matches a large gap in the few-level spectrum, e.g., $(\pi/3,\pi)$ for $n=1/3$ [Fig. 1(a)] or

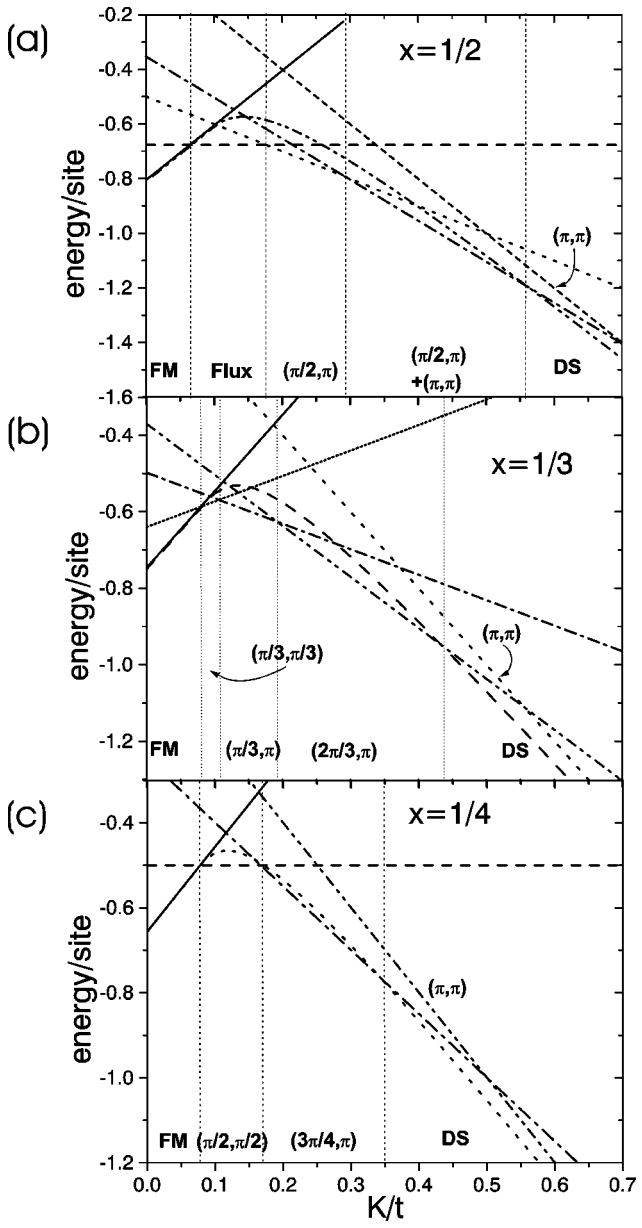

FIG. 3. Energies of selected spin configurations for $n=1/2$ (a), $n=1/3$ (b), and $n=1/4$ (c) at all values of K/t. Note in (a) the clear succession of the ground state with increasing K/t from flux phase to $(\pi/2,\pi)$ to $(\pi/2,\pi)+(\pi,\pi)$. Note in (b) the competition of several phases around $K/t=0.1$, and in (c) the dominance of the phase $(\pi/2,\pi/2)$ at intermediate K/t.

$(\pi/2,\pi/2)$ for $n=1/4$ [Fig. 1(b)]. The calculation of the kinetic part for the double-spiral phase follows the 2D case above, with reduction of the bandwidth by a factor of $\cos\Theta/2$, while the magnetic part varies as $\cos\Theta$. We do not find that canted states are favored in these considerations. Finally, two special configurations which require separate consideration are the $(\pi/2,\pi)+(\pi,\pi)$ phase, to which we return in Fig. 10, and flux phases.

Flux phases[26] are an important feature of the model in any dimension higher than 1. From Eq. (2) it is clear that the hopping term also contains a phase factor, and that for certain spin textures this phase may differ depending on the path through the lattice taken between two points. The simplest flux phase is that appearing at half-filling over a broad range of intermediate K/t, as discussed in Ref. 24, and shown in the snapshot in Fig. 9(c) below. The term ''flux phase'' is used here to refer to any spin configuration with this nontrivial topological property, which can be quantified by a nonzero spin current.[24] In principle, a variety of flux phases may exist, but we have not yet been able to find any others which are ground states at any filling. At the analytical level, the semimetallic density of states[26] of the dispersion

$$\epsilon_{\mathbf{k}}=\pm\sqrt{\cos k_x^2+\cos k_y^2} \tag{6}$$

of the simplest flux phase, which is zero precisely at half filling, accounts for its particularly low energy at $n=1/2$. We will characterize this phase in detail in Sec. V.

While these classical, zero-temperature pictures turn out to be rather valuable, and also not quantitatively unreasonable, for understanding the 2D pictures to follow, they are limited by the imagination of the authors as further possibilities may not be excluded. We have obtained many of the phases proposed in Fig. 3 in MC simulations, and the following Figs. 4–6 illustrate some representative results.

In Fig. 4 is shown $S(\mathbf{k})$, histogram and snapshot information for a phase at filling $n=1/2$ and for the ratio $K/t=0.22$. We see a single peak in $S(\mathbf{k})$ [Fig. 4(a)] only at $(\pi/2,\pi)$, indicating an island phase of FM pairs (the ''islands'') arranged in an AF pattern. The histogram [Fig. 4(b)] shows essentially only angles of 0 and π, ruling out a possible interpretation as a $\pi/2$ spiral in one direction; the ratios of angles 0 to angles π is approximately 1:3 as expected. Finally, the instantaneous spin configuration in Fig. 4(c) illustrates that the simulation has in fact converged quite well to the expected phase. Comparison with Fig. 3(a) indicates that for the 2D case, the value of K/t for a robust $(\pi/2,\pi)$ phase is that expected from the infinite system at $T=0$.

Figure 5 illustrates the same quantities for filling $n=1/3$ and $K/t=0.25$. For this relatively large parameter ratio, the dominant $(2\pi/3,\pi)$ phase in $S(\mathbf{k})$ [Fig. 5(a)] consists of AF chains with spin configuration $\uparrow\uparrow\downarrow\uparrow\uparrow\downarrow\uparrow\uparrow\downarrow\cdots$.[3] This is one of the primary types of island phase which we will mention again in Secs. IV and V. Both parts of Fig. 5 show in addition that this phase is not pure in the small-system MC simulation, with spin misalignments across the cluster manifest as residual components in $S(\mathbf{k})$. As in Fig. 4(b), the histogram (omitted) shows an absence of intermediate angles from any kind of spiral phase.

Figure 6 characterizes the phase arising for $n=1/4$ at $K/t=0.20$. From Fig. 3(c) we expect the phase $(3\pi/4,\pi)$ as ground state, and indeed this is the dominant component in $S(\mathbf{k})$ [Fig. 6(a)]. The rather stronger admixture of other components arises because the chosen value of K/t is close to a phase crossover, and so other possible 8×8 phases are not entirely absent. These are not reflected in the histogram (not shown) because all the pure phases present have angles of only 0 or π, but the snapshot [Fig. 6(b)] does show a small amount of misalignment between the predominantly AF-oriented spins. We note that the expected pure configuration (see below Fig. 3) remains rather hard to observe in Fig.

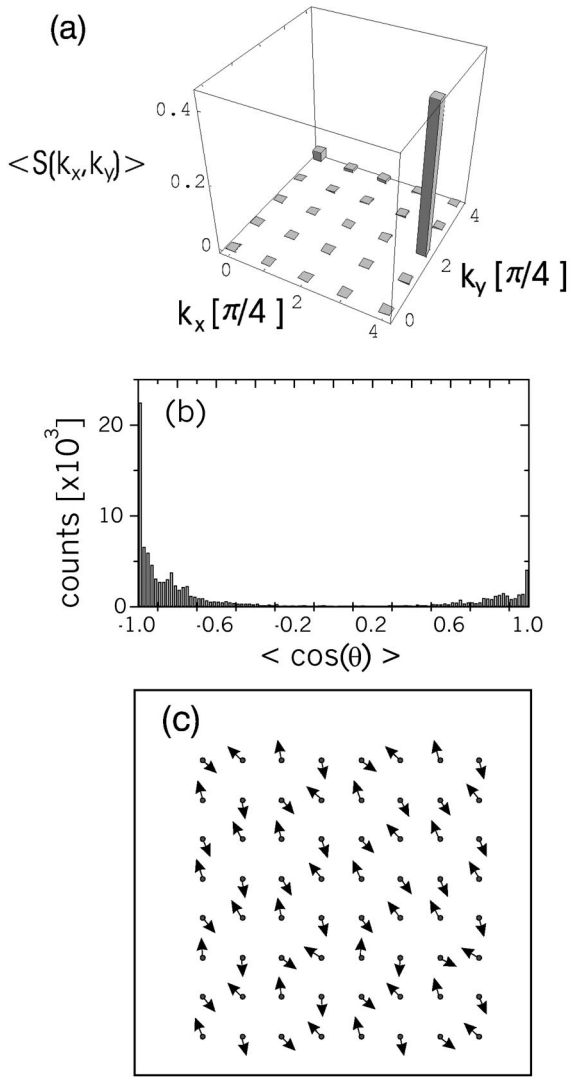

FIG. 4. MC phase for $n=1/2$ at $K/t=0.22$, calculated for an 8×8 system. (a) Structure factor. (b) Angle histogram. (c) Configuration snapshot.

6(b), and ascribe this to the mixing problem, and to the effects of fluctuations on the small-cluster MC calculation. This example illustrates both the need for careful consideration of finite-size effects, and the fact that for all commensurate fillings there exist regions of K/t (close to the line crossings in Fig. 3) where the MC results show strong mixtures of different phases. We note in passing that for all fillings we find pure FM phases at small but finite K/t ratios, in accord with zero-temperature, infinite-system expectations based on Fig. 3. These straightforward cases are not shown here. At large values of K/t, small-cluster calculations are unable to access the double spiral phase, and show instead the AF. We defer a more detailed characterization of the most interesting phases in these figures, namely the flux phase at $n=1/2$, the $(\pi/3,\pi)$ phase at $n=1/3$, and the $(\pi/2,\pi/2)$ phase at $n=1/4$, until Sec. V, after addressing the question of phase separation.

The results of Figs. 4 –6 were obtained for small systems, where finite-size effects are of paramount importance. For

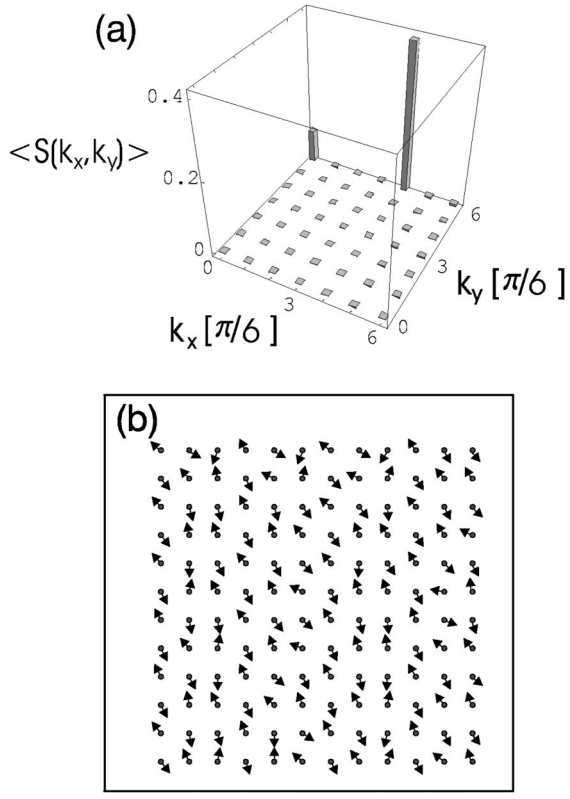

FIG. 5. MC phase for $n=1/3$ at $K/t=0.25$, calculated for a 12×12 system. (a) Structure factor. (b) Configuration snapshot.

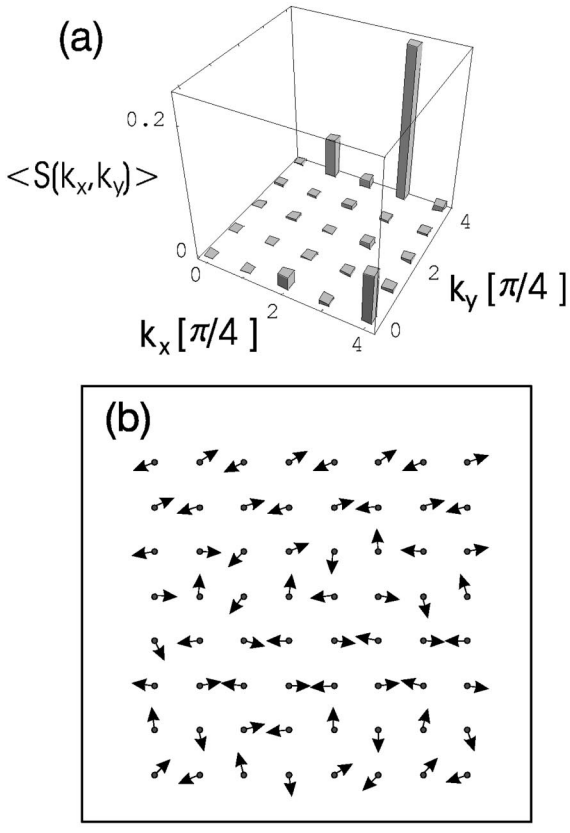

FIG. 6. MC phase for $n=1/4$ at $K/t=0.20$, calculated for an 8×8 system. (a) Structure factor. (b) Configuration snapshot.

fillings $n=1/2$ and $n=1/4$ we may compare 4×4 with 8×8 MC results, and for $n=1/3$ 6×6 with 12×12. These comparisons give already a good indication of where, for example, certain of the many possible phases are anomalously favored by the location of the chemical potential relative to a gap between sets of degenerate states. Even more valuable information is provided by comparison with the infinite-system results: these may be augmented by performing the same calculation, placing spins in a fixed configuration and deducing the magnetic and kinetic energies, for the system sizes 4×4 to 12×12 of the simulations (and further for 16×16). An effective calibration of the MC results is then possible, by which is meant a renormalization to account for effects arising only from system size, which is particularly important in discussing phase transitions (Sec. V).

On these finite systems we are unable to observe phase transitions, which are replaced by crossovers occurring in a finite range of K/t. As we will show in Sec. V, however, a certain amount of care is required in interpreting two-peak features in $S(\mathbf{k})$, because some robust, single phases arising at particular values of filling and K/t do indeed have more than one characteristic wave vector in small systems. Another feature requiring particular attention is the possibility of large-unit-cell phases, which cannot be accessed in the MC simulations. An example already mentioned is the double spiral, which is expected from Fig. 3 to be the most favorable phase on approaching the AF limit, into which this phase in fact passes continuously. However, at intermediate to large values of K/t we must also consider a competing, large-unit-cell (large-m) phase of the type $((m-k)\pi/m,\pi)$, $k\ll m$, with only 0 and π angles between the spins, in which the kinetic energy gain comes from spins shared between rare FM pairs in an otherwise AF structure. These phases are compared in the next section.

To conclude this section, we find that island-like phases are quite ubiquitous at all intermediate values of K/t (Fig. 3). The FM islands may be restricted in one direction, giving rise to stripelike features, or in both to give true islands, depending on the filling. These states are also accompanied by flux phases, of nontrivial spin texture, in certain parameter regimes. These novel, homogeneous phases arise only as a result of the competition between the first and last terms in Eq. (1), without recourse to additional physics (a discussion of which is deferred to a later section). However, we have worked in a canonical ensemble and considered only the energy of the emerging phases at zero or the lowest temperatures. We now turn to the question of phase separation within the model.

IV. PHASE SEPARATION

In the previous section we have considered a canonical ensemble, meaning fixed particle number, and deduced the ground states on the basis of minimal internal energy (or free energy at very low temperature). To ensure the global stability of these phases we must consider the possibility of their separation into regions of distinct and different filling. This propensity has been shown in the same model applied in 1D,[20] by working in a grand canonical ensemble and observing discontinuities in filling on varying the chemical potential. Here we choose to characterize phase separation from the energy in the canonical ensemble, by observing the curvature of this quantity as a function of filling. In Fig. 7 is shown the energy for fillings n between 0 and 1/2, at low, intermediate, and higher values of K/t. We note that the energy is a symmetrical function for $1/2\leqslant n\leqslant 1$ by electron-hole transformation, and do not comment further on this region. In these figures are included data from 12×12 and 16×16 systems, and infinite-system values for the flux and double spiral phases.

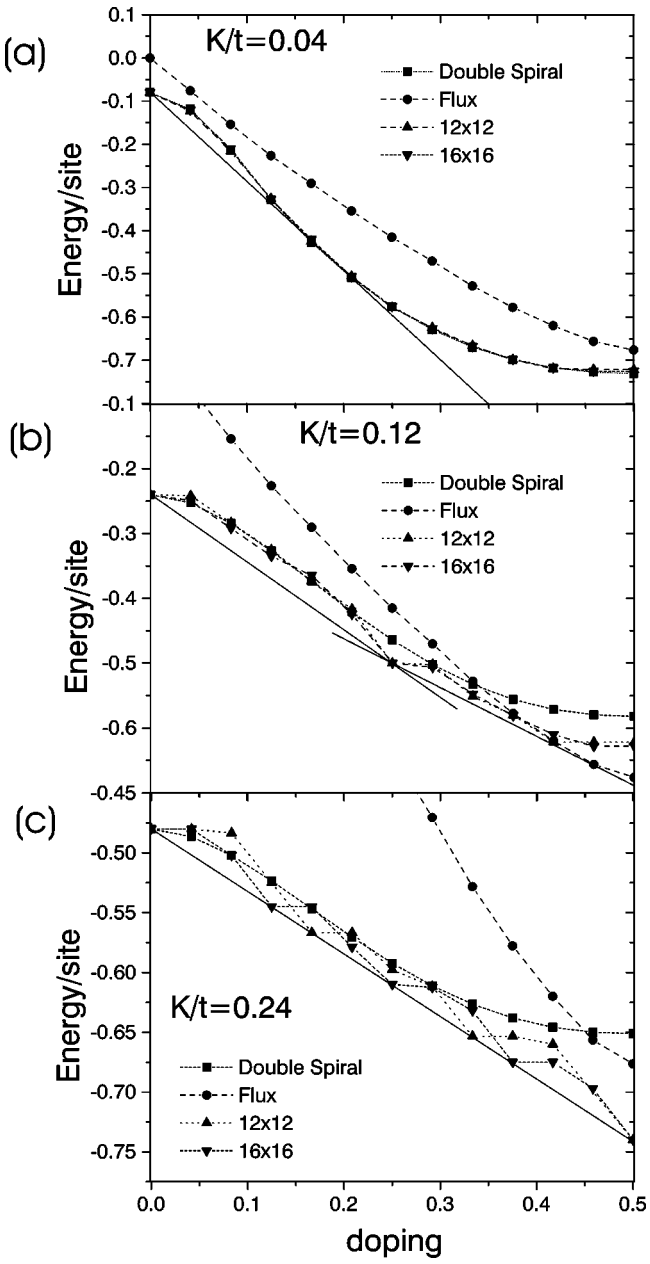

FIG. 7. Energy as a function of filling at fixed $K/t=0.04$ (a), $K/t=0.12$ (b), and $K/t=0.24$ (c) for a variety of phases. In (a), the tangent to the curve indicates the regime of phase separation by the Maxwell construction. Solid lines in (b) are Maxwell constructions. Solid line in (c) is a guide to the eye.

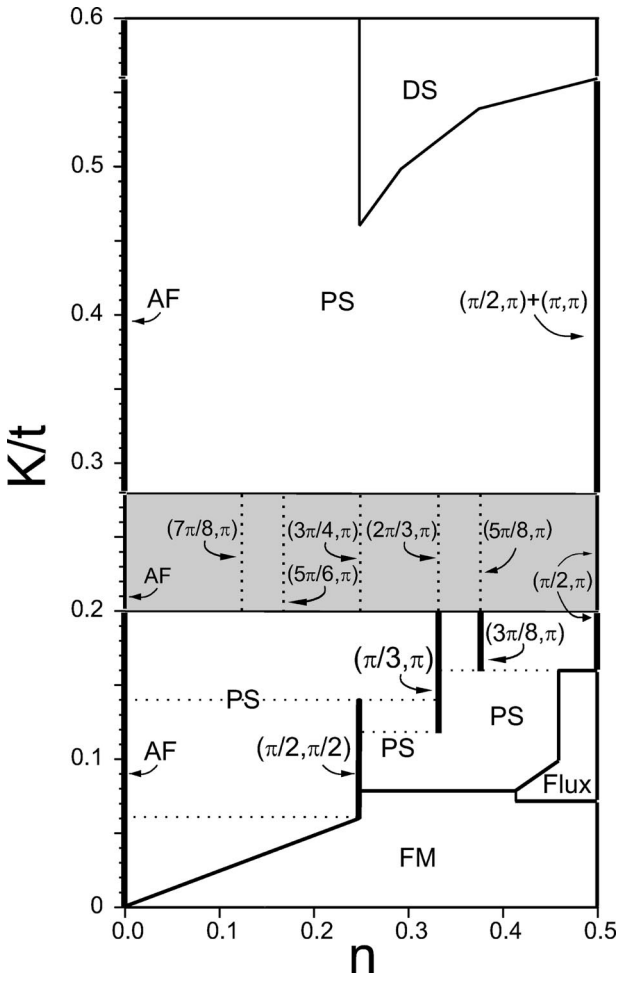

FIG. 8. Phase diagram of augmented FKLM for the full range of filling n and ratio K/t. PS denotes phase separation, the thick, vertical lines the island phases, and the shaded region the regime of large-unit-cell phases.

In Fig. 7(a) we see a convex (up) region at low filling, the implication of which is a preference for phase separation into two regions, one of zero hole content and the other whose filling n is given by a Maxwell construction using the tangent to the concave part of the curve. The empty region would have AF spin configuration, while for this low value of K/t the partially filled region would be FM. This result confirms that phase separation is an important property of the model, and agrees qualitatively with Ref. 20. In the absence of Coulomb interaction terms, on which we comment further in Sec. V, a complete separation into just two domains is expected; in the presence of Coulomb interactions, the separation should proceed to a characteristic length scale determined by their strength.[3,22,27]

For intermediate K/t [Fig. 7(b)] the situation is more complex. The convex regime extends over a much broader range of filling, but the ''curve'' is much less smooth, as a result of the particularly favorable island phases which can be established at the commensurate fillings. In fact, Maxwell constructions applied to Fig. 7(b) yield for this value of K/t a separation only into phases $n=0$ and 1/4, or into $n=1/4$ and n close to 1/2. Inspection of Fig. 3 shows that for $K/t=0.12$ the phases at these two fillings are particularly robust, whereas at $n=1/3$ a crossing between two phases occurs; by contrast, an $n=1/3$ phase would be expected as an end point of such separation for $K/t=0.15$, and indeed emerges (Fig. 8, below). This result highlights the dominant role of the commensurately filled phases, and suggests both ''high-contrast'' and ''low-contrast'' phase separation. By this is meant in the former case the abrupt split into zero- and part-filled regions, and in the latter a finer phase separation for certain K/t where incommensurate fillings $1/4<n<1/2$ may undergo separation into regions with closely neighboring, more commensurate fillings. These statements are made systematic in the summary phase diagram presented as Fig. 8.

At large K/t [Fig. 7(c)] the picture changes again. Here the finite-system points for commensurate phases show the intriguing feature of lying on a straight line connecting zero- and 1/2-filling. These are the $((m-k)\pi/m,\pi)$ phases introduced above, for those values of m small enough for the unit cell to fit within the system studied. Simple consideration of fixed spin configurations suggests that, in principle, phases of arbitrarily large unit-cell size are possible, and their energies will fall on the same line. From above, the nature of these phases is an AF configuration of spin chains with k up-spin and k down-spin pairs contained in an otherwise AF system with unit-cell size $2m$. In a fully classical system there would be no phase separation with filling in the thermodynamic limit at large K/t, but instead a continuous evolution of the unit-cell dimension to accommodate the added charges. In fact the values of k and m are fixed rather simply by the filling n, because the phases of this type appearing as the ground state are $((1-n)\pi,\pi)$, and their energy is given from the number of FM pairs and AF bonds as

$$E=-2K+n(K-t) \tag{7}$$

per site. For the commensurate fillings $n=1/m=1/2$, 1/3, and 1/4, we recover the island phases of Fig. 3. These phases appear to have been overlooked in Ref. 20, although the authors were little concerned with the high-K regime.

Our conclusions are summarized in the global phase diagram of Fig. 8. The properties of the minimal form of the FKLM [Eq. (1)] fall broadly into four regions, determined largely by the ratio K/t of the super- and double-exchange energy scales. For the lowest values of K/t, the system separates into AF and FM phases. For small to intermediate ratios, $0.08<K/t<0.2$, there is large-scale phase separation into only the island phases appearing at the commensurate fillings $n=1/4$, 1/3, 3/8, and 1/2. An exception here is the flux phase, which occupies a finite doping region close to $n=1/2$. We note in passing that within our classical formulation, only the FM and flux phases offer the possibility of hopping of conduction electrons throughout the system; only these phases would have metallic properties, and all others will be insulating.

For intermediate ratios $0.2<K/t<0.28$ we find the large-unit-cell phases discussed above. The hierarchy of possible states exists across the full doping range only when no competing phase falls below the straight-line energy function [Fig. 7(c), Eq. (7)] for any filling, and it is this condition which sets the limits in K/t of the shaded region in Fig. 8. We have marked (vertical dashed lines) the small-m phases which are compatible with the finite clusters considered, but

stress again that from the present calculations we expect to find all phases of the form $((1-n)\pi,\pi)$ for the infinite system. All states in the shaded region are a form of two-site FM island phase, which would show charge-ordering peaks in $N(\mathbf{k})$ (Sec. V), while the small-m members at the commensurate fillings provide examples which may be studied on small clusters (Figs. 4–6). At intermediate to large values of K/t, the large-unit-cell phases are replaced by a wide region of ''high-contrast'' phase separation due to the extraordinary stability of the $(\pi/2,\pi)+(\pi,\pi)$ phase at $n=1/2$. We have found only this phase, which is considered in more detail in the following section, and the AF phase with zero filling, to be stable in this regime of K/t, but stress that we cannot fully exclude the possibility of similar $((m-k)\pi/m,\pi)+(\pi,\pi)$ phases at other commensurate fillings. A search for these is limited by the available cluster size, and remains a topic for future investigation. Finally, at large values of K/t we recover the conventional, spiral-ordered DS phase, which passes smoothly to an AF phase.

V. ISLAND PHASES

With the results of the previous section concerning phase stability and separation, we may now turn in more detail to the regime of interest for island phases. This is largely limited to the commensurate fillings $n=1/2$, 1/3, and 1/4, and to the parameter range $0.1<K/t<0.3$, which (Fig. 8) encompasses both the isolated phases which are PS end points, and the large-unit-cell phases. For $n=1/2$, this region is dominated first by the flux phase, shown in Fig. 9. In Fig. 9(a), we see the double-peak structure of $S(\mathbf{k})$ with equal weight in $(0,\pi)$ and $(\pi,0)$ components which is the hallmark[24] of this spin configuration. We stress that the real-space spin structure [Fig. 9(c)] of this uniform phase contains both components simultaneously and equally, and there is no sense in which these arise as a superposition of two degenerate states or domains. In the MC simulation the peaks in $S(\mathbf{k})$ can be seen to grow together towards the value of 0.5 in the pure state. Figure 9(b) provides a rare example of a phase where the angles between neighboring spins are distributed not around the FM and AF configurations, but around $\pi/2$; our distribution is narrower than that in Ref. 24 because of the larger lattice size employed. This spin configuration gives rise to a uniform charge distribution with no inhomogeneous ordering.

By contrast, for the same filling at larger K/t, it is possible to find inhomogeneous charge structures. The $(\pi/2,\pi)$ phase of Fig. 4 exists as an end point both of phase separation and of the large-unit-cell series (Fig. 8). In this structure, electrons are delocalized across every second bond, or equivalently every FM bond in the $\pi/2$ direction, and are much more weakly present on the alternate AF bonds. This simple picture implies a stripelike charge order with wave vector $(\pi,0)$, and the phase would give peaks in x-ray diffraction or electron microscopy experiments, which measure the charge distribution $n(\mathbf{r})$. However, because the charge density n_i is the same on all sites, there is no structure in the quantity $n(\mathbf{k})$, which is defined in Eq. (5) and readily calculated on a finite cluster. This situation arises only for periodicities $\pi/2$ in the spin structure factor; for all higher m values, $n(\mathbf{k})$ and $N(\mathbf{k})$ computed from the site charges are indeed suitable indicators of charge order. We note briefly here that by translational invariance one may in fact expect to find a linear superposition of equivalent island phases, with a uniform mean value of n_i, and a charge order discernible only in $N(\mathbf{k})$. In the classical MC simulations we have shown results only for one such phase, which is separated by thermal barriers from its degenerate counterparts.

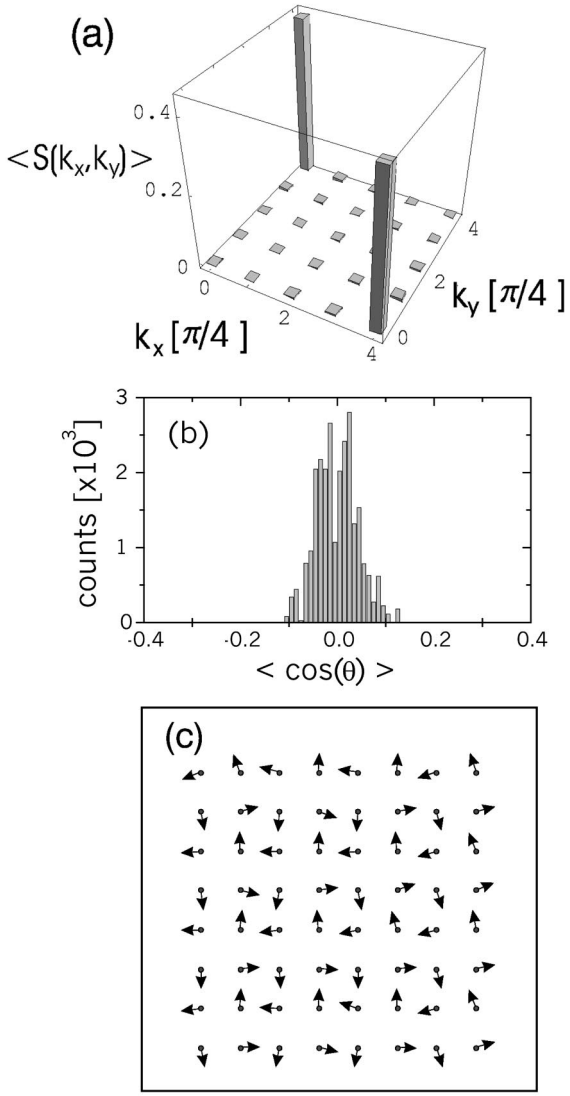

FIG. 9. MC results for $n=1/2$ at $K/t=0.12$, characterizing the flux phase on an 8×8 lattice. (a) Structure factor. (b) Angle histogram. (c) Configuration snapshot.

In Fig. 10 we show a further stable configuration, which we call the $(\pi/2,\pi)+(\pi,\pi)$ phase. As with the flux phase (Fig. 9) the two peaks in the structure factor shown in Fig. 10(a) do not indicate a mixture of phases. While the histogram information [Fig. 10(b)] can be used only to rule out intermediate angles, it is the instantaneous MC spin configuration [Fig. 10(c)] which reveals the true nature of this homogeneous phase. Once again one expects a 1D charge order

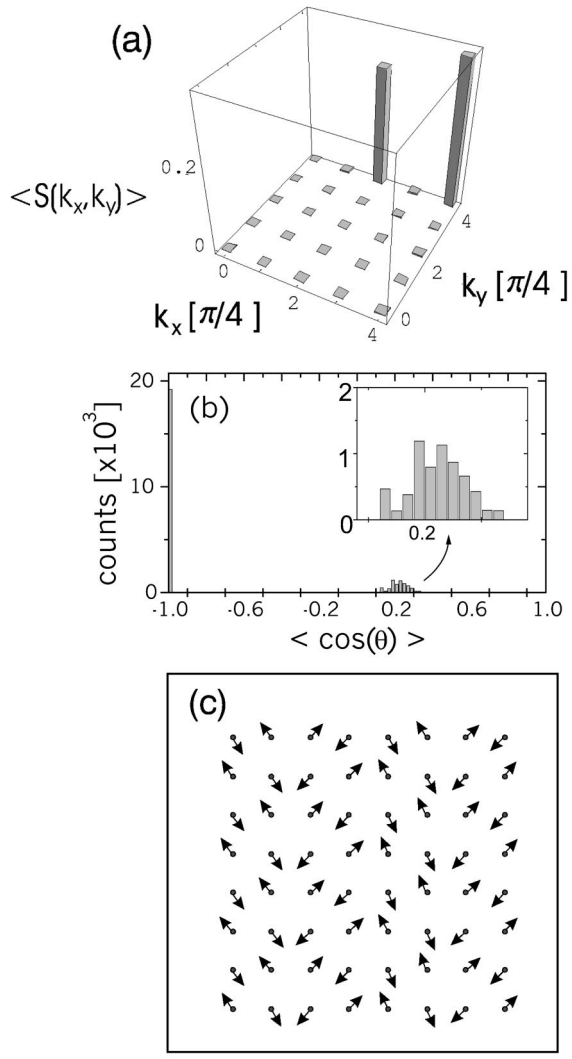

FIG. 10. MC results for $n=1/2$ at $K/t=0.32$, characterizing the $(\pi/2,\pi)+(\pi,\pi)$ phase on an 8×8 lattice. (a) Structure factor. (b) Angle histogram. (c) Configuration snapshot.

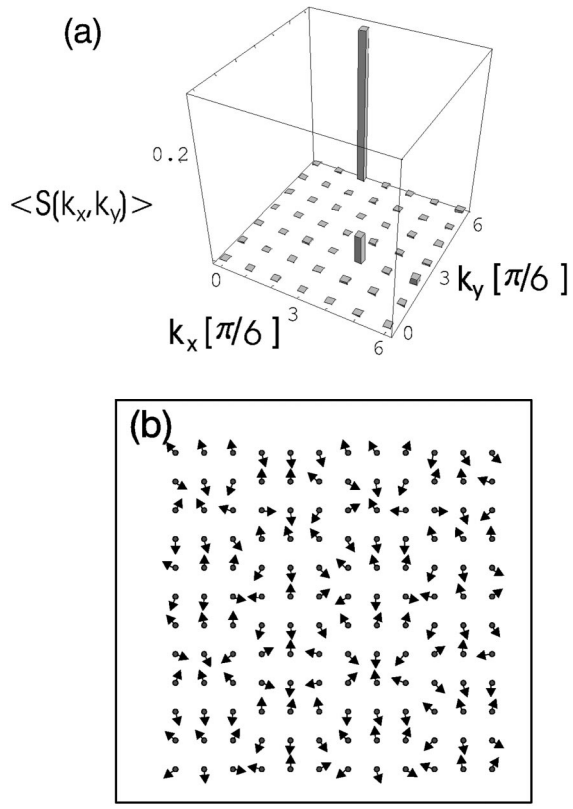

FIG. 11. MC phase for $n=1/3$ at $K/t=0.15$, characterizing the $(\pi/3,\pi)$ phase on a 12×12 system. (a) Structure factor. (b) Configuration snapshot.

for the same reasons as above. It is this phase, whose energy falls below the function given in Eq. (7) for $n=1/2$ and $K/t>0.28$, which breaks the large-unit-cell sequence, and is responsible for the wide region of high-contrast PS in the phase diagram of Fig. 8.

We dwell only briefly on the case of 3/8 filling. The results from the previous section show a $(3\pi/8,\pi)$ phase to be a stable end point in the PS regime, while the large-unit-cell region contains a $(5\pi/8,\pi)$ member. The properties of these configurations are readily deduced by comparison with the other examples presented, and both have charge-ordering wave vectors of $(\pi/4,0)$. Certain anomalies have been observed in experiment for filling $n=3/8$, but these appear to be restricted to 3D systems.

Turning to $n=1/3$, the most robust island phase in the intermediate parameter range is $(\pi/3,\pi)$, illustrated schematically in Fig. 1(a), and for $K/t=0.15$ in Fig. 11. At this value of K/t, Fig. 11(a) shows a rather strong $(\pi/3,\pi)$ peak, while the histogram (omitted) suggests a 1:2 ratio between FM and AF bond angles despite the weak presence of a $(\pi/3,2\pi/3)$ component. Figure 11(b) shows the actual spin structure, which gives rise to a charge order at the wave vector $(2\pi/3,0)$, due to the higher population of every third site in the $\pi/3$ direction. This ordering is present in the site charge distribution function n_i, which is shown in Fig. 12. From Fig. 12(a) it is clear that the charge contrast between the center and edge sites of each island approaches the classical ratio of 2:1.[3] Very similar results are obtained for the ''$((1-n)\pi,\pi)$'' phase $(2\pi/3,\pi)$ as K/t is raised beyond 0.2, as already shown in Fig. 5. In this state the charge-ordering wave vector remains $(2\pi/3,0)$. We have not been able to find a novel flux phase for 1/3 filling which might be a ground state anywhere in the intermediate K/t regime.

Finally, for $n=1/4$ the energy diagram [Fig. 3(c)] in the region of small to intermediate K/t is dominated by a single, and very robust, island phase. The extraordinary stability of the $(\pi/2,\pi/2)$ phase [Fig. 1(b)] at this filling is clear to see by diagonalizing the 4-site square cluster with hopping t. This exercise yields energy levels of $-2t,0,0,2t$, the location of the gaps demonstrating immediately why the phase so favors 1/4 filling, but is so unfavorable at $n=1/2$. Figure 13 requires little commentary, and we note only that the AF to FM angle ratio here is 1:1. As in Fig. 10, the charge-equivalence of all sites results in a homogeneous $n(\mathbf{k})$ [Eq. (5)], but the delocalization of charge within the 2×2 squares would give a peak at (π,π) in experiments measuring $n(\mathbf{r})$.

Returning to the question of phase transitions, these may

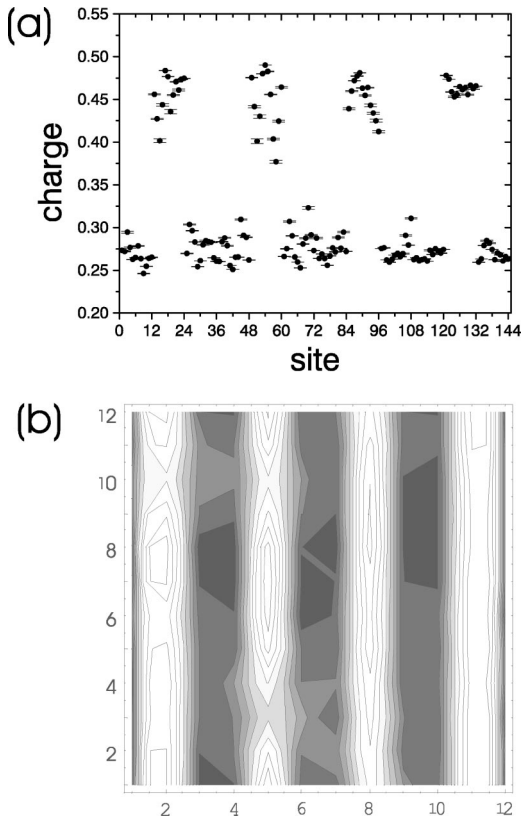

FIG. 12. Charge distribution function n_i for $n=1/3$ at $K/t=0.15$, illustrating charge order of $(\pi/3,\pi)$ phase on a 12×12 system. (a) Site charge densities: site numbers 1–12 label the first column from bottom to top [see (b) and Fig. 11(b)], 13–24 the second column from bottom to top, and so on. (b) Charge contour plot: high densities in white, low in gray.

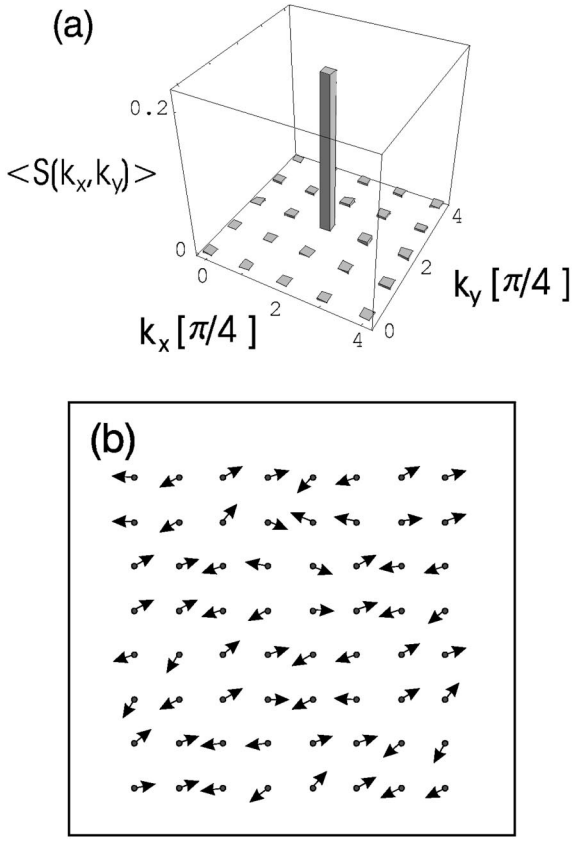

FIG. 13. MC phase for $n=1/4$ at $K/t=0.12$, characterizing the $(\pi/2,\pi/2)$ phase on an 8×8 lattice. (a) Structure factor. (b) Configuration snapshot.

be considered as a function of K/t or as a function of filling. In the former case the results are essentially those of Fig. 3. The only robust phases preceeding those in Figs. 9, 11, and 13 are FM phases, and at higher K/t a short cascade of further states leads to the AF configuration. As described in Sec. III, the phases arising from MC simulations require a renormalization of their final energies to account for system size, and when this is performed the crossovers are fully consistent with the infinite-system results. In the experimentally more relevant case of fixed K/t and variable filling, the results of Sec. IV imply that, for all but the smallest values of K/t, ''transitions'' take the form of a differential occupation of undoped and commensurately filled states, with the exception of the regime $0.2<K/t<0.28$ where they are replaced by a continuous evolution in the period of a large-unit-cell phase.

Returning to the experiments presented in the introduction, our results justify certain, rather broad conclusions. Manganite systems which are structurally layered, or have a 2D electronic structure as a result of orbital ordering in the cubic system, may indeed be susceptible to the island-phase phenomena, with resultant charge and spin order, discussed here. The effect of interlayer double-exchange and superexchange terms is rather involved: while weak interactions are invoked to discuss the stability of 2D phases in the true, 3D lattice, strong interactions give rise to a new phase diagram for the 3D system,[25] containing a rich variety of states which includes generalized island, flux and skyrmion configurations. The fundamental ingredient for this is only the competition between K and t intrinsic to all materials in the class. However, we have emphasized throughout the crude nature of the model we consider, and close with a brief discussion of the possible extensions which may be required to reproduce more closely the physics of real materials.

One of the fundamental features of manganite systems is the doubly degenerate nature of the e_g orbital. This has been included by a number of authors, and has been argued[28] to be essential in accounting for the CE-type (planar in 3D) charge order observed in $La_{1-x}Sr_xMnO_3$.[7] A further important ingredient in manganite systems is Jahn-Teller distortion of the local structural environment of each Mn ion,[29] which may act to lift the e_g orbital degeneracy, and also to promote charge order. Both terms have been included in a classical MC study of the type performed here,[21] albeit on very small systems. Island phases, in the orbital or spin degrees of freedom, were not among the already very rich variety of phases considered. When two e_g orbitals are considered, on-site Coulomb interactions were found[30] to lead to the formation of an upper Hubbard band, and to cause significant spectral weight shifts and broadening. As mentioned in Sec. IV, another term in many models of strongly correlated electrons is

a possible Coulomb repulsion between nearest-neighbor sites, conventionally denoted as V. This contribution acts to suppress phase separation, and to promote a charge ordering when V competes with the hopping energy scale t, as noted in the 1D system.[3] In higher dimensions, sufficiently strong V may lead to anisotropic charge order if the hopping is anisotropic, and more generally for weak V one expects a moving of phase boundaries to favor homogeneous states such as the stripes and islands considered here. Precisely this physics was found in Ref. 22, where the terminology ''island phase'' is applied to mean a shrinking of the size of phase-separated regimes. We stress that the island phases and charge order in our study are intrinsic to the physics of the competing double exchange and superexchange, and that an additional V term is not required for their appearance.

Finally, one of the major restrictions of the current approach is the limitation to small system sizes, which become smaller still on addition of the further terms discussed in the previous paragraph, and then still to largely classical considerations. The method of classical MC with diagonalization of the one-electron problem is in fact not particularly sophisticated, and we highlight here only two rather recent contributions which have the potential to reveal many more features on systems large enough to be considered thermodynamically representative. These are the variational mean field[31] and hybrid Monte Carlo[32] techniques, both introduced for the double-exchange problem by the same group of authors, which allow extensions in the former case to 96^3 systems with appropriate approximations, and in the latter to 16^3 sites with rather fewer. A last important point is the question of corrections to the above results due to the effects of quantum fluctuations. In 1D, it was found[3] that the boundaries between phases were moved to significantly larger values of K/t than predicted classically. While the methods presented herein do little to allow an assessment of fluctuation effects, these should be significantly smaller in 2D, both directly because of the higher dimensionality, and because the 1D results were obtained with a localized (t_{2g}) spin $S=1/2$, whereas the classical limit may be no less representative of the physical situation ($S=3/2$). Thus our phase diagrams can be expected to be qualitatively quite accurate. One may also ask if quantum fluctuations would act to destroy the coherence of the large-unit-cell phases: because these phases are not spiral-ordered, and already possess the AF or FM local spin alignment favored by fluctuations, they may be assumed to be robust in this respect.

VI. SUMMARY

In conclusion, we have considered the possibility of ''island'' phases and associated charge order in 2D systems, using as a model the augmented FKLM with strong Hund coupling. Indeed we find that stripelike and island phases are stable at intermediate values of K/t for each of the commensurate fillings $n=1/2$, 1/3, and 1/4. This result includes stability against global phase separation, even in the absence of additional Coulomb terms. Spiral magnetic order appears near the antiferromagnetic regimes at low filling or at large K/t. A variety of ''flux'' phases is possible, because the electron phase factor is nontrivial in all dimensions $d>1$, but we find only one to be a stable ground state and this at $n=1/2$. While the flux phase has a homogeneous charge distribution, the majority of the island phases show a charge modulation. Thus even the simple form (1) of the FKLM reproduces some of the most important experimental features of manganite charge and spin order. The critical values of K/t for transitions between ordered phases, and between ordered and separated phases, may be identified rather accurately from classical considerations augmenting small-system studies.

ACKNOWLEDGMENTS

We are grateful to A. Aligia, C. Balseiro, C. Batista, D. Garcia, K. Held, and D. Poilblanc for helpful discussions. This work was supported by the Consejo Nacional de Investigaciones Cientificas y Tecnicas (CONICET) of Argentina, and by the Deutsche Forschungsgemeinschaft through Grant No. SFB 484 (B.N.). We acknowledge also the support of program ECOS-SETCIP A97EO5 for bilateral cooperation between France and Argentina.

[1] E. D. Wollan and W. C. Koehler, Phys. Rev. **100**, 545 (1955).
[2] C. Zener, Phys. Rev. **82**, 403 (1951); P. W. Anderson and H. Hasegawa, *ibid.* **100**, 675 (1955).
[3] D. J. Garcia, K. Hallberg, C. D. Batista, M. Avignon, and B. Alascio, Phys. Rev. Lett. **85**, 3720 (2000).
[4] C. T. Chen and S.-W. Cheong, Phys. Rev. Lett. **76**, 4042 (1996).
[5] Y. Yamada, O. Hino, S. Nohdo, R. Kanao, T. Inami, and S. Katano, Phys. Rev. Lett. **77**, 904 (1996).
[6] J. M. de Teresa, M. R. Ibarra, P. A. Algarabel, C. Ritter, C. Marquina, J. Blasco, J. Garcia, A. de Moral, and Z. Arnold, Nature (London) **386**, 256 (1997).
[7] S. Mori, S.-W. Cheong, and C. T. Chen, Nature (London) **392**, 473 (1998).
[8] W. Bao, J. D. Axe, C. H. Chen, and S.-W. Cheong, Phys. Rev. Lett. **78**, 543 (1997).
[9] H. L. Liu, S. L. Cooper, and S.-W. Cheong, Phys. Rev. Lett. **81**, 4684 (1998).
[10] Y. Tomioka, A. Asamitsu, H. Kuwahara, Y. Moritomo, and Y. Tokura, Phys. Rev. B **53**, R1689 (1996).
[11] H. Kawano, R. Kajimoto, H. Yoshizawa, Y. Tomioka, H. Kuwahara, and Y. Tokura, Phys. Rev. Lett. **78**, 4253 (1997).
[12] W. Bao, C. T. Chen, S. A. Carter, and S.-W. Cheong, Solid State Commun. **98**, 55 (1996).
[13] Y. Moritomo, A. Nakamura, S. Mori, N. Yamamoto, K. Ohoyama, and M. Ohashi, Phys. Rev. B **56**, 14 879 (1997).
[14] Y. Murakami, H. Kawada, H. Kawata, M. Tanaka, T. Arima, Y. Moritomo, and Y. Tokura, Phys. Rev. Lett. **80**, 1932 (1998).
[15] J. Q. Li, Y. Matsui, T. Kimura, and Y. Tokura, Phys. Rev. B **57**, R3205 (1998).
[16] E. Müller-Hartmann and E. Dagotto, Phys. Rev. B **54**, R6819

(1996).
[17] J. Riera, K. Hallberg, and E. Dagotto, Phys. Rev. Lett. **79**, 713 (1997).
[18] J. L. Alonso, L. A. Fernandez, F. Guinea, V. Laliena, and V. Martin-Mayor, Phys. Rev. B **63**, 064 416 (2001).
[19] E. Dagotto, S. Yunoki, A. L. Malvezzi, A. Moreo, J. Hu, S. Capponi, D. Poilblanc, and N. Furukawa, Phys. Rev. B **58**, 6414 (1998).
[20] S. Yunoki and A. Moreo, Phys. Rev. B **58**, 6403 (1998).
[21] S. Yunoki, A. Moreo, and E. Dagotto, Phys. Rev. Lett. **81**, 5612 (1998).
[22] A. L. Malvezzi, S. Yunoki, and E. Dagotto, Phys. Rev. B **59**, 7033 (1999).
[23] Reviews of both theoretical and experimental studies are provided in E. Dagotto, S. Yunoki, and A. Moreo, in *Physics of Manganites*, edited by T. A. Kaplan and S. D. Mahanti (Plenum, Michigan, 1998); A. Moreo, S. Yunoki, and E. Dagotto, Science **283**, 2034 (1999).
[24] D. Agterberg and S. Yunoki, Phys. Rev. B **62**, 13 816 (2000).
[25] J. L. Alonso, J. A. Capitán, L. A. Fernandez, F. Guinea, and V. Martin-Mayor, cond-mat/0101390 (unpublished).
[26] M. Yamanaka, W. Koshibae, and S. Maekawa, Phys. Rev. Lett. **81**, 5604 (1998).
[27] J. Lorenzana, C. Castellani, and C. Di Castro, cond-mat/0010092 (unpublished).
[28] J. Van den Brink and D. Khomskii, Phys. Rev. Lett. **82**, 1016 (1998).
[29] M. Capone, D. Feinberg, and M. Grilli, Eur. Phys. J. B **17**, 103 (2000).
[30] K. Held and D. Vollhardt, Phys. Rev. Lett. **84**, 5168 (2000).
[31] J. L. Alonso, L. A. Fernandez, F. Guinea, V. Laliena, and V. Martin-Mayor, Phys. Rev. B **63**, 054411 (2001).
[32] J. L. Alonso, L. A. Fernandez, F. Guinea, V. Laliena, and V. Martin-Mayor, Nucl. Phys. B **596**, 587 (2000); cond-mat/0007450 (unpublished).